A 3D printed microfluidic flow-cell for microscopy analysis of *in situ*-grown biofilms

Mathilde Frost Kristensen,[a*] Dirk Leonhardt,[a] Merethe Louise Bønneland Neland,[b] Sebastian Schlafer[a]

[a]Department of Dentistry and Oral Health, Aarhus University, Vennelyst Boulevard 9, 8000 Aarhus C, Denmark.

[b]Department of Engineering, Science and Technology, Aarhus University. Inge Lehmanns Gade 10, 8000 Aarhus C, Denmark

E-mail addresses: sebastians@dent.au.dk (S. Schlafer), mfk@dent.au.dk (M.F. Kristensen), dirk.leonhardt@dent.au.dk (D. Leonhardt), 201609796@post.au.dk (M.L.B. Neland)

*Corresponding author: *Mathilde Frost Kristensen; Department of Dentistry and Oral Health, Aarhus University, Vennelyst Boulevard 9, 8000 Aarhus C, Denmark.*

Word count =4698 (including all tables, legends and references)

Abstract

Biofilm phenomena ranging from metabolic processes to attachment, detachment and quorum sensing are influenced by the fluid flow across the biofilm. A number of commercially available flow-cells allow for microscopy analysis of laboratory biofilms under flow, but there is a lack of shear controlled microfluidic devices that accommodate biofilms grown *in situ* on carriers or tissue samples. Therefore, we developed a flow-cell with adjustable geometry for microscopy analysis of *in situ*-grown biofilm samples under shear-controlled flow. The flow-cells were designed as one-piece disposable models, 3D-printed in resin and sealed with a coverslip after insertion of the biofilm sample. As a proof of concept, we studied the impact of stimulated saliva flow on pH developments in *in situ*-grown dental biofilms exposed to sucrose. Under static conditions, pH dropped in the biofilms, with pronounced differences between individual biofilms, but also between different microscopic fields of view within one biofilm. pH in the top layer of the biofilms tended to be lower than pH in the bottom layer. Under conditions of stimulated saliva flow (5 mm/min), pH rose to neutral or slightly alkaline values in all biofilms, and the vertical gradients were reversed, with the biofilm bottom becoming more acidic than the top. Hence, the present work demonstrates the importance of flow for the study of pH in dental biofilms.

Keywords: 3D-print; Biofilm; Confocal microscopy; Extracellular pH; Flow-cell; Microfluidic device

Abbreviations: FOV, field(s) of view

1. Introduction

Most natural and industrial biofilms form in the presence of a liquid flow, which affects all stages of biofilm formation, from the initial adhesion to maturation and the eventual detachment. With increasing flow and thus increasing shear stress, the total number of adhering cells has been shown to decrease, whereas the bonds formed by those bacteria that attach are more long-lived (Lecuyer et al. 2011)·(Dickinson and Cooper 1995). During maturation, the flow velocity and the nutrient concentration of the fluid constitute the main factors controlling biofilm growth. Cell clusters on the surface of the biofilm access nutrients more easily than cells in deeper layers, especially at low flow rates (Stewart 2012). Consequently, some colonies grow faster than others do, and this brings about the typical heterogeneous biofilm morphology with mushroom-shaped towers surrounded by clusters with limited height (Stewart 2012). Moreover, flow forms the biofilm mechanically, and episodes of elevated shear induce different degrees of elastic or plastic deformation. If the shear stress excesses the cohesive or adhesive strength of the biofilm, it will even lead to gradual or complete biofilm detachment (Stewart 2012).

Through its impact on nutrient supply and the clearance of metabolic products, flow also plays a vital role for regulatory processes in biofilms. Studies have shown that external flow influences the communication system quorum sensing (QS) by creating gradients in the concentration of autoinducers that set the outer layers of the biofilm in a QS-off mode and contribute to biofilm robustness (Vaughan et al.; Kim et al. 2016). Moreover, mathematical modelling has shown that under flow conditions, autoinducers accumulate downstream and in irregularly shaped areas of the biofilm, which further illustrates the complex interplay of flow and metabolism.

Despite the importance of flow for biofilm behavior, most biofilm studies are conducted under static conditions, on coupons, on tissue samples, or simply in well plates (Coffey and Anderson 2014). Mechanical shear is typically applied by dipping or rotary shaking, and nutrients are often supplied by daily medium changes (Coffey and Anderson 2014). While such static setups reduce the experimental workload and cost, they do not reflect natural biofilm growth conditions, and care must be taken to extrapolate findings from experiments performed without flow.

In the past decade, more attention has been drawn to the use of flow cells for biofilm growth that permit microscopy-based analyses (Rusconi et al. 2014). While some of these devices allow for shear-controlled flow conditions (Ong et al. 2017; Gianfranco Donelli 2014; van der Waal et al. 2017; Gulati et al. 2017; Rath et al. 2017; Gianfranco Donelli 2014) biofilms typically have to be grown inside the device, which precludes the use of biofilm samples grown in natural settings. In some flow chambers, a biofilm grown on a tissue or an industrial surface may be incorporated, but these solutions have a high purchase price and a limited size range. Most importantly, discrepancies between sample and chamber geometry hamper an optimal control of flow conditions.

Here, we present the design of a new, versatile flow-cell for microscopy that accommodates samples of different geometry and provides shear-controlled flow. The flow-cell is designed in dedicated 3D-software that allows easy adjustments of geometry to fit the sample in question. Subsequently, the disposable flow-cells are 3D-printed and ready to use. As a proof of concept, we collected dental biofilms grown *in situ* on custom-made glass slabs and demonstrated the use of the flow cells, as well as the tremendous influence of salivary flow on pH-developments inside the biofilms.

2. Materials and Methods

2.1 *In situ* biofilm growth. Biofilms were collected from a healthy volunteer (female, 23y) who had not used antibiotics during the last three months and showed no signs of active caries. An individual removable lower jaw splint was designed (3Shape Dental System; Copenhagen, Denmark) and fabricated (BEGO Bremer Goldschlägerei, Bremen, Germany) with a 3D-printed metallic core (Wirobond C; Bego Bremer Goldschlägerei) and acrylic buccal flanges. For intraoral biofilm growth, non-fluorescent custom-made glass slabs (size: 4x4x1.5 mm; surface roughness: 1200 grit; Menzel, Braunschweig, Germany) were mounted with sticky wax (Dentsply, Weybridge, UK) on the buccal flanges in a slightly recessed position to reduce mechanical interference with the soft tissues. The splint was worn for experimental periods of 96 hours during which it was immersed in 10 % sucrose solution 3 times per day for 2 min. Otherwise, the splint was worn at all times and only removed during oral hygiene procedures, meals and intake of liquid other than water. Prior to the experiments, the participant was provided with written and oral information about the study and informed consent was obtained. The protocol was approved by the Danish National Committee on Health Research Ethics (1-10-72-178-18).

2.2 Flow-cell design and production. The flow-cell was designed in the free software 123D-Design (Autodesk, San Rafael, USA) as a one-piece disposable model consisting of an inlet, a chamber with a viewing window and an outlet (Fig. 1). For pH analyses under flow, the geometry of the flow-cell was designed to fit the x and y dimensions of the glass slabs used for biofilm growth, with small margins of 0.2 mm and 0.05 mm to allow for easy insertion. The vertical dimension was set to 1.6 mm, yielding a flow space of 100 µm that matches the saliva film thickness in the oral cavity (Dawes et al. 1989). The resulting file was transferred to the printer-associated software Meshmixer (Autodesk, San Rafael, USA),

and the areas of the flow cell that needed support material to maintain the connection to the print basis were identified (Fig. 2A). Support material was automatically added in the Meshmixer software (Fig. 2B) and the flow cells were subsequently nested on the print basis (Fig. 2C, D). Hereafter, they were printed in resin (V-Print SG; Voco, Cuxhaven, Germany) using a SolFlex 650 3D printer (Voco). After printing, the flow-cells were cleaned in a reusable isopropanol ultrasound bath (BDH Chemicals, Radnor, USA) for 3 min, and then in a fresh isopropanol ultrasound bath for another 3 min. After air-drying, the cells were post-polymerized and vacuum treated for 15 min (3M, Minnesota, USA) to secure total curing and removal of the oxygen inhibition layer. Finally, the support material was removed manually before use.

2.3 Flow-cell assembly. A glass slab was mounted in the flow-cell with a drop of silicone (Extrude light-body; Kerr, Orange, USA) with the biofilm facing down. To obtain a realistic flow medium, the participant provided paraffin-stimulated saliva samples on the days of biofilm collection. The saliva samples were filtrated through sterile gauze, cleared by centrifugation (5 min, 1150 g) and used immediately. The outlet of the flow-cell was connected to a waste reservoir, the inlet to a 1 mL syringe (Henke Sass Wolf, Tuttlingen, Germany) filled with cleared saliva, sucrose (4 % w/V) and C-SNARF-4 (20 µM). The bottom of the flow-cell was subsequently sealed to a round coverslip (25 mm dia.; Hounisen, Skanderborg, Denmark) with instant adhesive (Renfert, Hilzingen, Germany) and placed in a cell chamber (Attofluor™; ThermoFisher Scientific, Waltham, USA) with cutouts milled in-house to accommodate the inlets. Finally, the syringe was mounted in a pump (TSE Systems 540060, Bad Homburg, Germany) and the cell chamber was placed in an adapter seated in a microscope heating stage (Heating Insert P Lab-Tek™, PeCon, Germany)..

2.4 Ratiometric pH measurements. The calibration of the ratiometric dye is described elsewhere (Schlafer et al. 2011). Briefly, buffered solutions of C-SNARF-4, adjusted to pH 4.5-8 in steps of 0.1 pH units, were imaged with a confocal microscope (Zeiss LSM 510 META) at 37 °C. Fluorescence was excited at 543 nm and detected from 576-608 nm (green channel) and 629-661 nm (red channel). After background subtraction, the ratios of the emissions in the two channels were plotted against pH and fitted to a calibration curve. For pH measurements in dental biofilms, images were acquired using the same microscope settings as during calibration. Image size: 364 x 364 pixels; pixel dwell time: 18.03 µsec; optical slice: 1.6 µm (2 Airy Units). At the beginning of an experiment, the medium was pumped into the flow-cell and three microscopic fields of view (FOV) were chosen at random. The distance from the biofilm top to the coverslip was measured to calculate the average cross sectional flow area. After 15 (t_{15}) and 30(t_{30}) min of static incubation with sucrose, images were acquired in two layers of each FOV, 5 µm from the top and bottom of the biofilm. Then the flow was turned on at a rate of 5 mm/min, which corresponds to the velocity of stimulated saliva in the oral cavity (Dawes and Dibdin 1986). Again, images were acquired 5 µm from the biofilm top and bottom, after 15 (t_{45}) and 30 min (t_{60}) of dynamic incubation. Background images with the laser turned off were taken regularly to correct for detector offset. The experiments were carried out in biological triplicates.

2.5 Digital image analysis. For calculation of extracellular pH, the red and green channel images were exported separately as TIF files. Background fluorescence was subtracted in ImageJ (Schneider et al. 2012), and the mean filter (pixel radius 1) was applied to compensate for detector noise. The brightest image of each layer in a FOV, typically the green channel image acquired at t_2, was segmented with a manually chosen intensity threshold that identified extracellular areas and excluded all bacteria. The selection was then converted to a region of interest (ROI) and transferred to all other images of the same

layer and FOV. Green channel images were divided by the corresponding red channel images resulting in a fluorescence ratio and a SD. Then, the ratios were converted to pH values according to equation (1):

$$\ln\left(\frac{1.61}{ratio-0.0937}-1\right)*0.397+6.12. \quad (1)$$

3. Results

The flow-cells consist of an inlet, an outlet and a well-defined insert to fit *in situ*-grown biofilm samples. The x, y and z dimensions of the insert can easily be adjusted in the design software to match samples with different geometry. For the present work, a size of 4.2 x 4.05 x 1.6 mm was chosen to accommodate the glass slabs used for biofilm growth (Fig.1). The bottom of the insert was left open, such that it turned into a viewing window for microscopy when sealed with a coverslip. Sample and chamber size resulted in a vertical flow space of 100 µm, which corresponds to the thickness of the saliva film in the mouth (Dawes et al. 1989). To avoid a sudden increase in resistance, inlet and outlet were designed to narrow down towards the insert, until reaching the same dimensions as the flow space. While the size of the glass slabs or any other carrier for biofilm growth can be standardized, the biofilm thickness may vary. We therefore measured the exact distance between the biofilm surface and the coverslip experimentally under the microscope to determine the cross sectional flow area and calculated the volumetric flow rate.

The flow-cells were printed as one-piece disposable models. Each print job took approximately one hour and yielded 20 flow-cells. If the flow-cells were nested on the printer basis as a stack, up to 150 flow-cells could be produced in one print job (Fig. 2). An optimal placement of flow-cells resulted in a material cost of approximately 0.7 euro per flow-cell printed with a precision of ±25µm (Voco).

As a proof of principle, we studied the impact of flow on pH developments inside *in situ* grown dental biofilms. Although all three examined biofilms derived from the same subject, their acidogenic potential differed markedly. After 15min of static incubation, average pH ranged from 6.1 to 6.9. After 30 min of static incubation, those differences had increased, with averages ranging from pH 5.7 to 6.9. Irrespective of the acidogenic potential of the biofilms, pH differed between individual FOV inside each biofilm, which confirms the presence of distinct microenvironments. The onset of flow had a dramatic impact on biofilm pH. In all three biofilms, average pH after was raised considerably after 15 min of flow, and the previously observed large differences in average pH had levelled out (range: 7.3 - 7.6). After 30 min of flow, average pH remained slightly alkaline in all biofilms, but still lower than the pH of the flow medium (typically 8.2). Likewise, differences between FOV inside the same biofilm were still present (Fig.3). Fig. 4 shows the pH development over time in a highly acidogenic FOV. Interestingly, flow had an impact on vertical pH gradients inside the biofilms, although they were very thin (25-35 µm). Under static conditions, pH tended to be lower in the top layer of the biofilms, in those biofilms that had a substantial acid production. With the onset of flow, the gradients were reversed, leaving the bottom layer more acidic than the top (Table 1).

Table 1

pH differences between top and bottom of the biofilm

Replicate	**ΔpH (t_{15}); [SD]**	**ΔpH (t_{30}); [SD]**	**ΔpH (t_{45}); [SD]**	**ΔpH (t_{60}); [SD]**
1	-0.24; [0.1]	-0.26; [0.06]	0.35; [0.21]	0.43; [0.07]
2	0.20; [0.11]	0.17; [0.07]	0.36; [0.3]	0.45; [0.26]
3	-0.07; [0.1]	-0.25; [0.16]	0.14; [0.01]	0.23; [0.17]

The effect of flow on vertical pH gradients in *in situ*-grown dental biofilms. For each replicate biofilm, the difference between pH at the biofilm top and bottom (ΔpH) is shown after 15 min (t_{15}) and 30 min (t_{30}) of static incubation with sucrose, as well as after 15 min (t_{45}) and 30 min (t_{60}) of dynamic incubation (5 mm/min). Under dynamic conditions, pH at the biofilm bottom became lower than pH at the biofilm top (ΔpH>0).

4. Discussion

The present work describes the development of an inexpensive 3D-printed microfluidic flow-cell with adaptable geometry, which allows studying *in situ* grown biofilm samples under shear-controlled conditions. We demonstrated the dramatic impact of medium flow on metabolic processes in dental biofilms by comparing pH developments in *in situ* grown dental biofilms under static and dynamic conditions.

There is a strong need to expand research on *in situ* grown biofilms, since processes observed in mono-species or even multi-species laboratory biofilms cannot be readily extrapolated to a clinical context (Malone et al. 2017). Mimicking the flow conditions of those real-life situations proves difficult, as there is a lack of microfluidic flow devices able to shear-control and that can be adjusted to a particular sample geometry (Rath et al. 2017; Klug et al. 2016; Duckworth et al. 2018). In fact, the present research was prompted by our fruitless efforts to establish a controlled flow across *in situ*-grown dental biofilm samples using a commercially available perfusion chamber (Warner instruments, Hamden, USA). With our newly developed 3D printed flow-cell, many of the limitations of conventional flow chambers can be overcome. Whatever the size of the biofilm sample in question, the geometry of the flow chamber can

211 be adapted accordingly in the design software and the flow space can be chosen to match *in situ*
212 conditions. With a known cross-sectional flow area, the flow velocity and the resulting shear force can
213 then be calculated precisely for a given volumetric flow rate (Young et al.) when small diameter tubings
214 are used, the flow-cell runs on minute amounts of liquid, which reduces the cost of long-term experiments
215 with expensive fluorescent dyes. In the present study, typical volumetric flow rates used to mimic saliva
216 flow were in the range of 2.0 µl/min. With a material price of less than one Euro and an increasing
217 availability of 3D printers, the use of custom-made flow-cells may soon become more widespread in
218 microbiological applications.
219 Compared to static setups, experiments involving flow are more laborious and require a higher amount
220 of dexterity. In the present study, the most intricate experimental steps were the placement of the glass
221 slab inside the flow-cell without touching the biofilm on the surface, as well as the sealing of the flow-
222 cell to the coverslip. While microfluidic devices may be particularly sensitive to clogging, it proved to
223 be no problem for the present work, despite the use of a rather viscous flow medium. Likewise, the
224 formation of bubbles was very limited, and we conducted all experiments without a bubble trap.
225 The printer used for additive manufacturing of the flow cells operated with a precision of ±25 µm (Voco).
226 Hence, there was a certain variation in the flow space below the biofilm, after assembly of the cells. We
227 therefore measured the distance between biofilm and cover slip with the help of the microscope for each
228 sample, before starting the flow, and adjusted the volumetric flow rate accordingly. In some instances,
229 the distance exceeded the working length of the objective, and the flow-cell had to be discarded.
230 The use of confocal microscopy for analysis of the biofilm samples entails a couple of limitations. First,
231 the penetration depth of the laser beam into a fluorescently labelled sample does typically not exceed 100
232 µm, which precludes the analysis of thick biofilms. Second, the flow space between cover glass and
233 biofilm increases the distance between objective and sample. If high magnifications are required for

analysis, as is the case for pH ratiometry, the vertical dimension may exceed the working distance of the employed objective. Finally, the increased distance between objective and biofilm reduces the contrast between cells and background, in particular if a dye like C-SNARF-4 is used that does not only target bacteria, but also stains the flow space. Hence, the current setup was close to the limit of feasibility for ratiometric pH analysis with C-SNARF-4. For other applications, like studying the effect of shear on biofilm deformation or disruption, the flow-cell setup may be less challenging.

Compared to previous work, the experimental setup of the present study mimics *in situ*-conditions more accurately (Schlafer et al. 2015; Schlafer and Dige 2016; Schlafer et al. 2011), providing a flow velocity and film thickness that match those present in the oral cavity (Dawes and Dibdin 1986; Dawes et al. 1989). Moreover, freshly collected saliva was used as the flow medium and all experiments were carried out at a physiological temperature.

The data demonstrate that 96-h smooth surface biofilms, collected from a caries-inactive volunteer, are not able to maintain acidic microenvironments under conditions of stimulated saliva flow, despite the continuous presence of sucrose. This finding is well in line with the results of Imfeld, whose telemetric experiments in healthy volunteers showed that plaque pH does not drop to critical values during the chewing of sugar-containing toffees (Imfeld 1983). With the help of pH ratiometry, we demonstrated that horizontal pH gradients inside biofilms, which have previously been observed under static conditions (Dige et al. 2016), persist after the onset of flow. Moreover, we showed that flow has a considerable impact on vertical pH gradients inside thin (25-35 µm) *in situ*-grown biofilms. The constant flow of a slightly alkaline saliva medium affects pH in the top layers of the biofilms more than in bottom layers. Hence, our findings corroborate the results of a previous study conducted on a five-species laboratory model of dental biofilm (Schlafer *et al.* 2018). Future experiments will investigate the effect of different flow rates on pH in biofilms of different age in a larger subject group and contribute to our understanding

of the caries process. In conclusion, the newly designed microfluidic flow cell proves to be a valuable tool for microscopy analyses of *in situ*-grown biofilm samples under flow conditions.

Figure 1. Computer design and 3D-printed flow-cell. A1, B1) The flow-cell model in the design software. The flow-cells consist of an inlet, a bottomless viewing chamber and an outlet. The entrance to the viewing chamber is designed with a funnel shape to ensure fluid flow across the entire sample. **A2, B2)** The flow-cell after 3D print. Flow-cells are printed with a precision of ±25 µm. The supporting material has been removed manually with rotating instruments. Bars = 4 mm.

Figure 2. Addition of support material and nesting of the flow-cell in the printer software. The printer software identifies the areas of the flow cell that need support material to maintain the connection to the print basis, areas shown in red (**A**). The support material is added automatically (**B**) and the flow-cells are nested on the printer basis (**C**, **D**). Bars = 4 mm

Figure 3. pH developments inside dental biofilms under static and flow conditions. pH was monitored ratiometrically in three replicate biofilms (**A**, **B** and **C**) for 60 min after exposure to sucrose. After 30 min of static incubation, the biofilms were exposed to a flow rate of 5 mm/min, corresponding to stimulated saliva flow in the oral cavity (arrows). Each line shows the pH development in one microscopic field of view (FOV). Measurements from the biofilm surface are displayed in black, recordings from the biofilm bottom in grey. Under static conditions, pH dropped in all biofilms, although at different rates in different biofilms and FOV. pH at the surface was lower than pH at the biofilm bottom. With the onset of flow, the pH rose to neutral or slightly alkaline values in all biofilms. Vertical pH gradients were reversed, whereas horizontal gradients inside the biofilms persisted. Error bars = SD.

Figure 4. Color visualization of extracellular pH in one microscopic field of view of a dental biofilm. Panel **A**) shows the biofilm stained with C-SNARF-4, prior to the removal of the bacteria. The contrast between bacterial cells (bright) and biofilm matrix (dark) is sufficient for subsequent image analysis. In panels **B**, **C**, **D** and **E**, the cells were removed, pH in the extracellular space was calculated and false coloring was applied to visualize pH levels. Under static conditions, average pH in the FOV dropped to 6.53 after 15 min (**B**) and to 5.35 after 30 min (**C**). After 15 min and 30 min of flow, average pH in the FOV rose to slightly alkaline values (15 min: 7.17; 30 min 7.1). Bars = 20 µm.

Funding

This work was supported by the Danish Dental Association.

Declarations of interest:

The authors have nothing to declare.

Acknowledgements

The authors would like to thank Lene Grønkjær and Javier E. Garcia for excellent technical support.

Publication bibliography

Coffey, Barbara M.; Anderson, Gregory G. (2014): Biofilm formation in the 96-well microtiter plate. In *Methods in molecular biology (Clifton, N.J.)* 1149, pp. 631–641. DOI: 10.1007/978-1-4939-0473-0_48.

Dawes, C.; Dibdin, G. H. (1986): A theoretical analysis of the effects of plaque thickness and initial salivary sucrose concentration on diffusion of sucrose into dental plaque and its conversion to acid during salivary clearance. In *Journal of dental research* 65 (2), pp. 89–94. DOI: 10.1177/00220345860650021701.

Dawes, C.; Watanabe, S.; Biglow-Lecomte, P.; Dibdin, G. H. (1989): Estimation of the velocity of the salivary film at some different locations in the mouth. In *Journal of dental research* 68 (11), pp. 1479–1482. DOI: 10.1177/00220345890680110201.

Dickinson, Richard B.; Cooper, Stuart L. (1995): Analysis of shear-dependent bacterial adhesion kinetics to biomaterial surfaces. In *AIChE J.* 41 (9), pp. 2160–2174. DOI: 10.1002/aic.690410915.

Dige, Irene; Baelum, Vibeke; Nyvad, Bente; Schlafer, Sebastian (2016): Monitoring of extracellular pH in young dental biofilms grown in vivo in the presence and absence of sucrose. In *Journal of oral microbiology* 8, p. 30390.

Duckworth, Peter F.; Rowlands, Richard S.; Barbour, Michele E.; Maddocks, Sarah E. (2018): A novel flow-system to establish experimental biofilms for modelling chronic wound infection and testing the efficacy of wound dressings. In *Microbiological research* 215, pp. 141–147. DOI: 10.1016/j.micres.2018.07.009.

Gianfranco Donelli (2014): Microbial biofilms. Methods and protocols. Springer protocols: Humana Press (http://www.springer.com/series/7651), checked on 2014.

Gulati, Megha; Ennis, Craig L.; Rodriguez, Diana L.; Nobile, Clarissa J. (2017): Visualization of Biofilm Formation in Candida albicans Using an Automated Microfluidic Device. In *Journal of visualized experiments : JoVE* (130). DOI: 10.3791/56743.

Imfeld T.N (1983): 3. Intraoral pH Telemetry in Man Materials and Methods. In Thomas N. Imfeld (Ed.): Identification of low caries risk dietary components, vol. 11. Basel, London: Karger (Monographs in Oral Science, vol.11), pp. 9–48.

Kim, Minyoung Kevin; Ingremeau, Francois; Zhao, Aishan; Bassler, Bonnie L.; Stone, Howard A. (2016): Local and global consequences of flow on bacterial quorum sensing. In *Nature microbiology* 1, p. 15005. DOI: 10.1038/nmicrobiol.2015.5.

Klug, Barbara; Santigli, Elisabeth; Westendorf, Christian; Tangl, Stefan; Wimmer, Gernot; Grube, Martin (2016): From Mouth to Model. Combining in vivo and in vitro Oral Biofilm Growth. In *Frontiers in microbiology* 7, p. 1448. DOI: 10.3389/fmicb.2016.01448.

Lecuyer, Sigolene; Rusconi, Roberto; Shen, Yi; Forsyth, Alison; Vlamakis, Hera; Kolter, Roberto; Stone, Howard A. (2011): Shear stress increases the residence time of adhesion of Pseudomonas aeruginosa. In *Biophysical journal* 100 (2), pp. 341–350. DOI: 10.1016/j.bpj.2010.11.078.

Malone, Matthew; Goeres, Darla M.; Gosbell, Iain; Vickery, Karen; Jensen, Slade; Stoodley, Paul (2017): Approaches to biofilm-associated infections. The need for standardized and relevant biofilm

methods for clinical applications. In *Expert review of anti-infective therapy* 15 (2), pp. 147–156. DOI: 10.1080/14787210.2017.1262257.

Ong, Louis Jun Ye; Islam, Anik; DasGupta, Ramanuj; Iyer, Narayanan Gopalakkrishna; Leo, Hwa Liang; Toh, Yi-Chin (2017): A 3D printed microfluidic perfusion device for multicellular spheroid cultures. In *Biofabrication* 9 (4), p. 45005. DOI: 10.1088/1758-5090/aa8858.

Rath, Henryke; Stumpp, Sascha Nico; Stiesch, Meike (2017): Development of a flow chamber system for the reproducible in vitro analysis of biofilm formation on implant materials. In *PloS one* 12 (2), e0172095. DOI: 10.1371/journal.pone.0172095.

Rusconi, Roberto; Garren, Melissa; Stocker, Roman (2014): Microfluidics Expanding the Frontiers of Microbial Ecology. In *Annu. Rev. Biophys.* 43 (1), pp. 65–91. DOI: 10.1146/annurev-biophys-051013-022916.

Schlafer, Sebastian; Dige, Irene (2016): Ratiometric Imaging of Extracellular pH in Dental Biofilms. In *Journal of visualized experiments : JoVE* (109). DOI: 10.3791/53622.

Schlafer, Sebastian; Garcia, Javier E.; Greve, Matilde; Raarup, Merete K.; Nyvad, Bente; Dige, Irene (2015): Ratiometric imaging of extracellular pH in bacterial biofilms with C-SNARF-4. In *Applied and environmental microbiology* 81 (4), pp. 1267–1273. DOI: 10.1128/AEM.02831-14.

Schlafer, Sebastian; Raarup, Merete K.; Meyer, Rikke L.; Sutherland, Duncan S.; Dige, Irene; Nyengaard, Jens R.; Nyvad, Bente (2011): pH landscapes in a novel five-species model of early dental biofilm. In *PloS one* 6 (9), e25299. DOI: 10.1371/journal.pone.0025299.

Schneider, Caroline A.; Rasband, Wayne S.; Eliceiri, Kevin W. (2012): NIH Image to ImageJ. 25 years of image analysis. In *Nature methods* 9 (7), pp. 671–675.

Stewart, Philip S. (2012): Mini-review. Convection around biofilms. In *Biofouling* 28 (2), pp. 187–198. DOI: 10.1080/08927014.2012.662641.

van der Waal, S. V.; Almeida, J. de; Krom, B. P.; Soet, J. J. de; Crielaard, W. (2017): Diffusion of antimicrobials in multispecies biofilms evaluated in a new biofilm model. In *International endodontic journal* 50 (4), pp. 367–376. DOI: 10.1111/iej.12634.

Vaughan, Benjamin L.; Smith, Bryan G.; Chopp, David L.: The Influence of Fluid Flow on Modeling Quorum Sensing in Bacterial Biofilms. In *Bull. Math. Biol.* 72 (5), pp. 1143–1165. DOI: 10.1007/s11538-009-9485-8.

Voco: SolFlex 170_350_650. The Industrial Grade DLP Dental 3D Printers SolFlex 650 ' 350 ' 170. voco.dental (Folders). Available online at https://www.voco.dental/us/portaldata/1/resources/products/folders/us/VC_84_009100_US_1018_SolFlex_brochure_web.pdf.

Young, Donald F.; Munson, Bruce R.; Okiishi, Theodore H.; Huebsch, Wade W.: Fundamentals of Fluid Mechanics. manual. 6th ed. 8 volumes. United States of America: Don Fowley. Available online at https://www.wileyplus.com/, checked on 2009.

Fig. 1

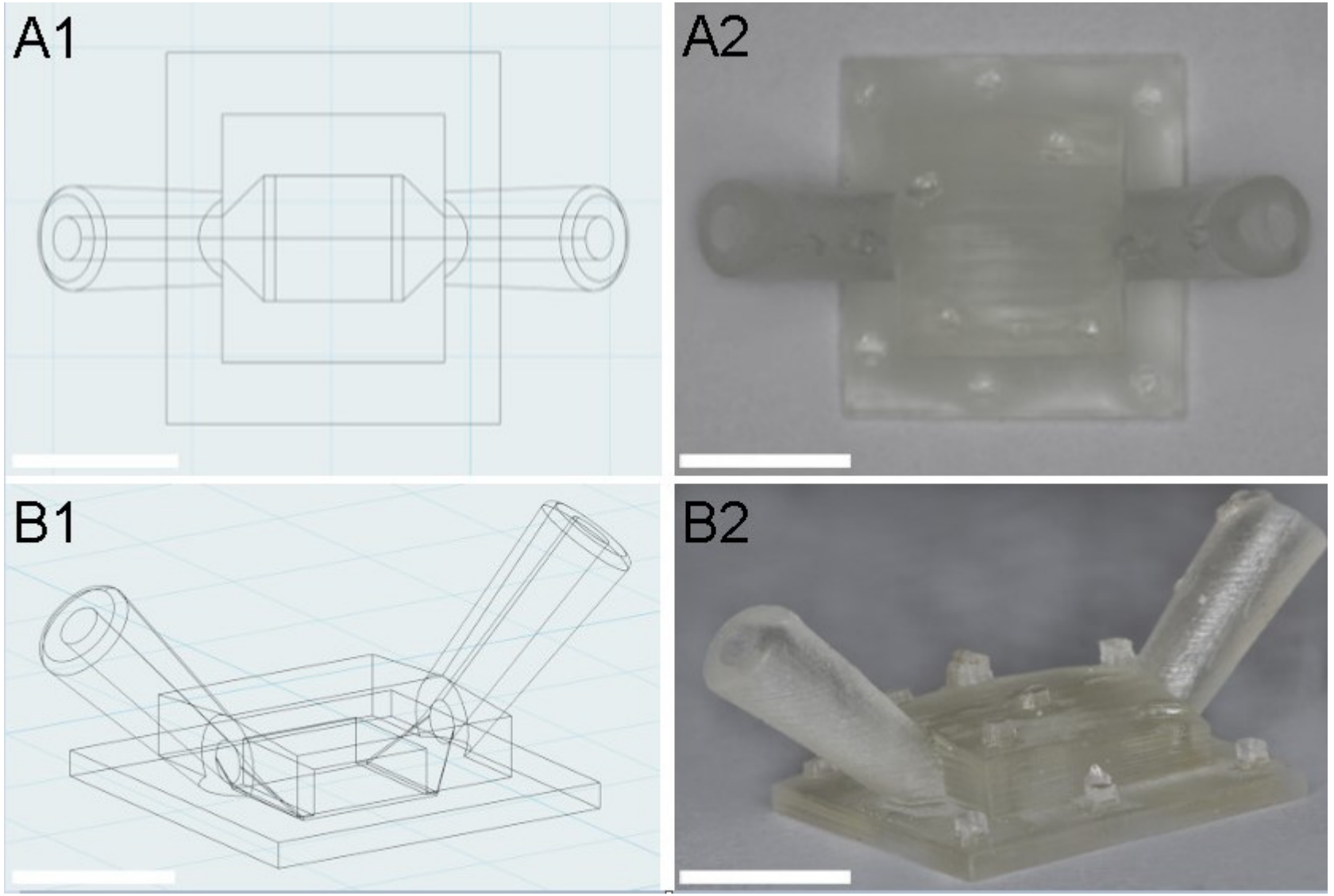

Fig. 2

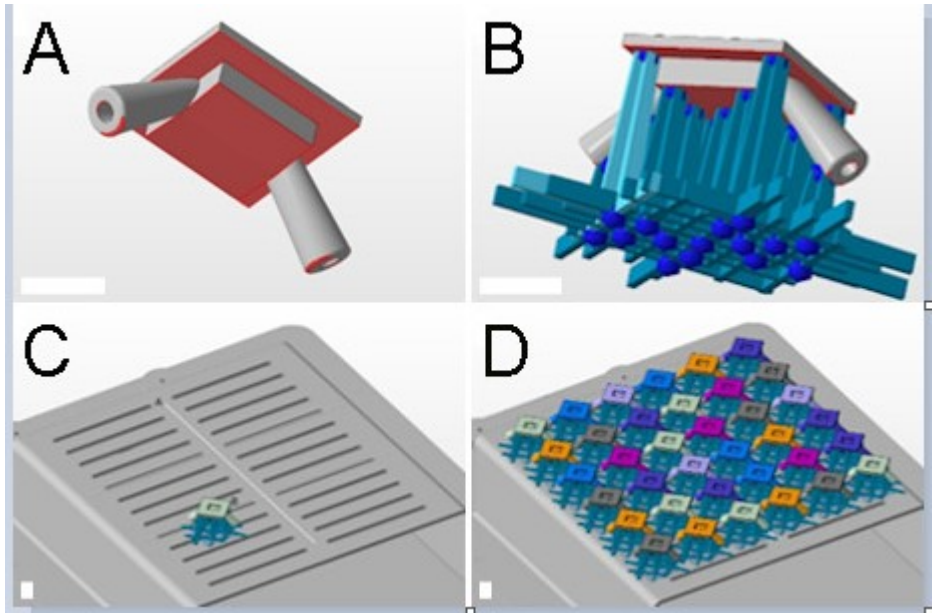

Fig. 3

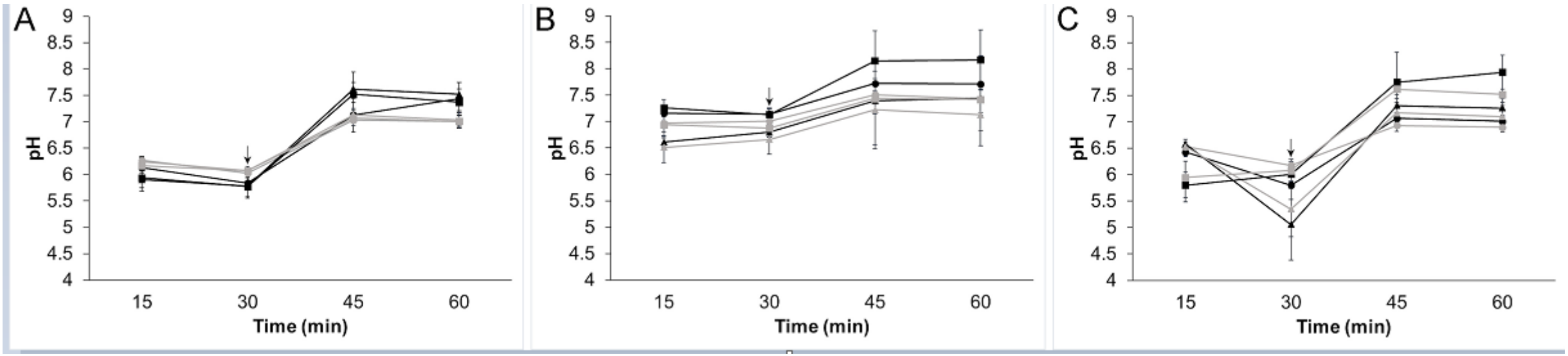

Fig. 4